Probing Z-Z' mixing at future e^+e^- colliders

A. A. Pankov*
International Centre for Theoretical Physics, Trieste, Italy
and Istituto Nazionale di Fisica Nucleare, Sezione di Trieste, Italy

N. Paver
Dipartimento di Fisica Teorica, Università di Trieste, Trieste, Italy
and Istituto Nazionale di Fisica Nucleare, Sezione di Trieste, Italy
(Received 14 September 1992)

We discuss the possibility of obtaining constraints on Z-Z' mixing from studies of the process $e^+e^-\to W^+W^-$ at planned high energy e^+e^- colliders, and derive the corresponding limits on the Z' mass for different extended models. Our results indicate that the limits on the mixing angle are quite stringent, and can typically reach the level of 10^{-5}–10^{-6}. We also present a detailed comparison with the potential of the reaction $e^+e^-\to f\bar{f}$, which shows that significantly better sensitivity to Z-Z' mixing should be expected from W^+W^- production.

PACS number(s): 14.80.Er, 12.15.Cc, 12.15.Ji, 13.10.+q

I. INTRODUCTION

Numerous extended theories have been proposed and deeply studied, either as viable extensions of the standard model incorporating it, or as alternatives to the model itself in the description of electroweak interactions. A common feature of most extended schemes is the prediction of the existence of one (or more) neutral heavy gauge bosons Z', whose mass and possible mixing with the standard Z reflect the Higgs structure of the theory [1]. From the phenomenological point of view there has been intense activity to formulate strategies for determining the Z' parameters from experimental data, and thus to test these theories. One approach is based on the search for direct Z' production at hadronic colliders and supercolliders [Fermilab Tevatron, Superconducting Super Collider (SSC), and CERN Large Hadron Collider (LHC)], with a discovery limit of $M_{Z'}\leq 3$–6 TeV (for E_6 models). The other approach is based on the study of the possible indirect effects of Z' bosons in e^+e^- annihilation at KEK TRISTAN, the CERN e^+e^- collider LEP, and at the planned Next Linear Collider (NLC), Japan Linear Collider (JLC), etc., which might be sensitive to Z' boson masses up to about 4 TeV [2–4].

In this regard, most attention has been given to the annihilation

$$e^+ + e^- \to f + \bar{f} \tag{1}$$

at LEP 1, leading to restrictions on the Z-Z' mixing angle, from which lower limits on $M_{Z'}$ could be derived, competitive with those obtained from the direct search at the Tevatron collider [5–8].

With the increased e^+e^- energy available at planned machines, stronger restrictions on the mixing angle will be allowed in principle by the measurement of the reaction [9]

$$e^+ + e^- \to W^+ + W^- \ . \tag{2}$$

The advantage of this process is that, in this case, deviations of cross sections from the standard model strongly increase with the total e^+e^- energy, as compared to transition (1), so that enhanced sensitivity to indirect Z' effects can be obtained even for fixed luminosity.

Thus, a possible scenario concerning this kind of search is represented in Fig. 1. Starting with reaction (1), at TRISTAN (with $\sqrt{s} < M_Z$) one can, in general, only obtain limits on $M_{Z'}$, because here the leading Z' effect is related to the γ-Z' interference instead of the small mixing angle [10,11], while from the line shape near the Z peak ($\sqrt{s}\approx M_Z \pm \Gamma_Z/2$) we can study Z-Z' interference [12]. At the Z peak (LEP 1), where the Z-exchange diagram dominates, limits of the Z-Z' mixing angle are derived from high precision measurements and can be turned into lower limits on the Z' mass in the different models [5,6,8]. At higher energies the situation of TRISTAN repeats, until possibly (and hopefully) reaching the Z' peak, where mass and couplings of the Z' could be measured and, depending on the precision, the mixing could be either established or limited through models [13].

Turning to reaction (2), at the energies typical of the NLC (500 GeV or greater), even off the Z' resonance peak one can place stringent bounds on Z-Z' mixing, stronger than those derived at the Z, due to the mentioned enhancement mechanism of the mixing effect in the interferences mediated by the Z exchange diagram [9]. Eventually reaching the Z' boson peak, the cross section for process (2) (proportional to the square of the mixing angle) is certainly smaller than for process (1), and the corresponding statistics are poorer. Nevertheless, as we will see in the sequel, in this case the enhancement mechanism also helps in improving the sensitivity to the

*Permanent address: Department of Physics, Gomel Polytechnic Institute, SU-246 746 Gomel, Belorussia, CIS.

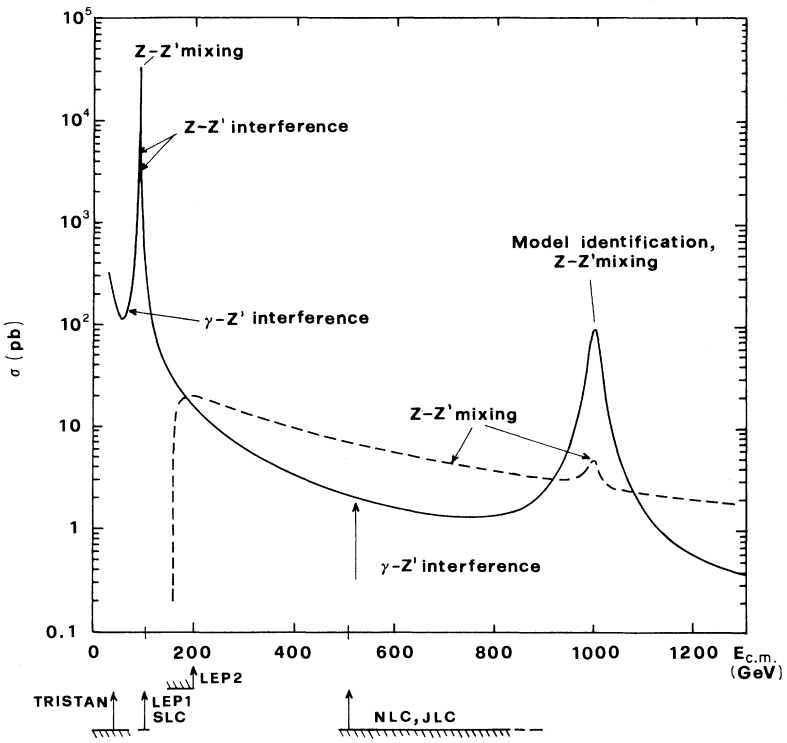

FIG. 1. Total cross sections of $e^+e^- \rightarrow$hadrons (solid line) and $e^+e^- \rightarrow W^+W^-$ (dashed line) vs energy. Z' from E_6 (χ model) with $M_{Z'}=1$ TeV and a Z-Z' mixing angle of 3×10^{-3} rad.

mixing angle by a large factor. Moreover, near-resonance observables for (2) have the potential of additional improvements, compared to on-resonance ones, essentially because γ-Z', ν-Z', and Z-Z' interference terms in the cross section are, in this case, linear in the mixing angle.

In the present paper we wish to discuss the above points, systematically analyzing the various possibilities offered by reaction (2), with reference to future experiments at energies reached at the NLC (or higher), and also comparing them with the potential of reaction (1). The plan of the paper is the following. In Sec. II we review in some detail the physical origin of the enhancement mechanism of indirect Z' effects in process (2). In Sec. III we discuss off-resonance strategies to obtain bounds on the mixing angle and the Z' mass from this reaction, and present the corresponding implications for extended models, specifically the left-right models (LRM's) [14], the alternative left-right models (ALRM) [15], and the E_6 models [1]. In Sec. IV we emphasize the significance of cross-section measurements on- and near-Z' resonance, and compare the results for the various extended models, obtained in this case, to those found in Sec. III. In Sec. V we discuss the potential of process (1) in establishing limits on the mixing angle, and compare it with process (2). Finally, some concluding remarks are given in Sec. VI.

II. CROSS SECTIONS AND ENHANCEMENT MECHANISM

As is well known [16–18], process (2) is described in the standard model (SM) by the diagrams of Fig. 2(a), mediated by photon, neutrino, and Z exchanges, which we denote respectively by A_γ, A_ν, and A_Z. Let us assume that some new physics induces a small departure of these amplitudes from the SM prediction and, for the moment, consider the case where only A_Z is changed by an energy-independent amount ϵ_Z:

$$A_Z \rightarrow (1+\epsilon_Z)A_Z \ , \tag{3}$$

leaving the other ones unchanged. As we will see below, ϵ_Z will be proportional to the Z-Z' mixing angle $|\phi| \ll 1$.

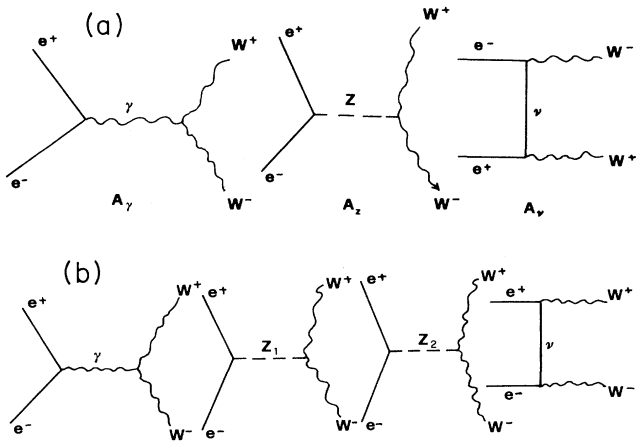

FIG. 2. Feynman diagrams for $e^+e^- \rightarrow W^+W^-$ in the SM (a) and in extended models (b).

We can introduce the quantity

$$\Delta_Z=\frac{\sigma(\epsilon_Z)-\sigma^{\rm SM}}{\sigma^{\rm SM}} \tag{4}$$

as an observable of the effect from new physics. In Eq. (4), by σ we may denote either the differential cross section $d\sigma/d\cos\theta$ or the integrated one, $\int_{z_1}^{z_2} d\sigma/d\cos\theta$, with θ the c.m. angle between the outgoing W^- and the e^- beam directions. Cross sections will be proportional to

$$\begin{aligned}&\sigma(\epsilon_Z)\sim|A_\gamma+A_\nu+(1+\epsilon_Z)A_Z|^2\ ,\\&\sigma^{\rm SM}\sim|A_\gamma+A_\nu+A_Z|^2\ .\end{aligned} \tag{5}$$

Accordingly, the right-hand side of (4) can be written to first order in ϵ_Z as [9]

$$\Delta_Z=\Delta_{1Z}+\Delta_{2Z}\ , \tag{6}$$

where

$$\begin{aligned}&\Delta_{1Z}=\epsilon_Z^0(R_{\gamma Z}+R_{\nu Z}+2R_{ZZ})\ ,\\&\Delta_{2Z}=\epsilon_{\gamma Z}R_{\gamma Z}+\epsilon_{\nu Z}R_{\nu Z}+2\epsilon_{ZZ}R_{ZZ}\ .\end{aligned} \tag{7}$$

In Eqs. (6) and (7) we take into account that, in general, ϵ_Z might consist of a part ϵ_Z^0 independent of the helicity structure of A_Z and of a part, made of ϵ_{iZ}, which has such a dependence. Moreover, the notation is such that

$$\begin{aligned}&R_{ij}=\sigma_{ij}/\sigma\ ,\\&\sigma\equiv\sigma^{\rm SM}=\sum_{i,j}\sigma_{ij}\quad(i,j=\gamma,\nu,Z)\ .\end{aligned} \tag{8}$$

The explicit expressions of σ_{ij} and of σ are reported in Appendix A for both the differential and the integrated cross sections. In Fig. 3 we separately represent the energy behaviors of σ_{ij} and of σ in the case of total cross sections. Differential cross sections have qualitatively the same behavior.

Referring to Fig. 3, the important feature of the partial contributions to the SM cross section, determined by σ_{iZ} (and, in general, by σ_{ij}), is their fast increase with the c.m. energy, essentially proportional to s/M_W^2, so that each term by itself would violate unitarity [16–19]. As is well known, the source of such divergences is the amplitude for producing a pair of longitudinally polarized $W^\pm$. In contrast, the cross section σ (total or differential), resulting from the sum of those contributions, decreases with the c.m. energy due to a delicate gauge cancellation among the different diverging terms. Consequently, the absolute values of R_{iZ} (and in general of R_{ij}), defined in Eq. (8) as ratios of increasing σ_{ij} and decreasing σ, have a significant rise with energy. For example, for the total integrated cross sections we have the asymptotic behavior [16–18] of

$$\sigma\propto\ln(s/M_W^2)/(s/M_W^2)$$

for $s\gg 4M_W^2$. In this case

$$R_{ij}\propto\frac{(s/M_W^2)^2}{\ln(s/M_W^2)}\ . \tag{9}$$

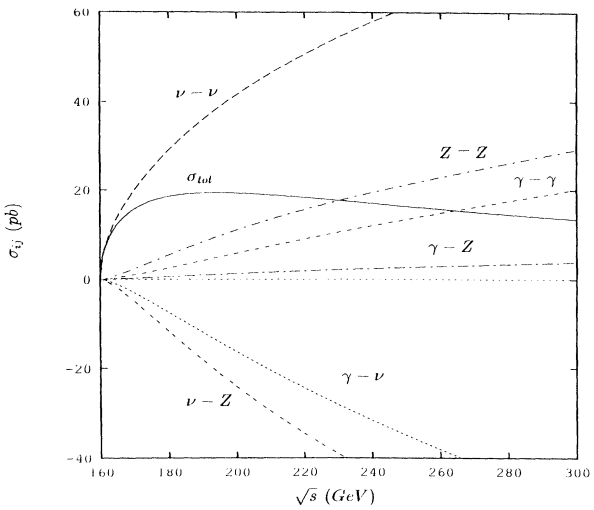

FIG. 3. SM total cross section of $e^+e^-\to W^+W^-$ and separate contributions vs energy.

From Eqs. (6) and (7), Δ_Z is a linear combination of the functions R_{iZ} with coefficients ϵ_Z^0 and ϵ_{iZ}, so that it also steeply increases with s. Indeed, although the R_{ij} have different signs, there is not complete compensation in the combinations of Eq. (7), so that the energy behavior of Δ_Z remains that of the R_{ij}. As anticipated in the previous section, this mechanism determines quite a significant enhancement of the sensitivity of process (2) to small effects from new physics (ϵ_Z) when the energy becomes very large, much larger than the W-pair production threshold. In fact, comparing the deviation from the SM cross section Δ_Z to the relative statistical uncertainty on the cross section $\delta\sigma/\sigma\sim 1/\sqrt{\sigma L_{\rm int}}$, as a consequence of the behaviors mentioned above, the sensitivity $\Delta_Z/(\delta\sigma/\sigma)$ increases with energy even at fixed time integrated luminosity $L_{\rm int}$.

Qualitatively, the same enhancement mechanism discussed above for the unpolarized total cross section works also in the cases of the differential cross section and for any kind of initial e^+e^- polarizations. A convenient set of formulas, and a more detailed discussion, can be found, e.g., in Ref. [9].

The range of $\sqrt{s}$ values for which we should expect the most significant manifestations of the above enhancement mechanism is the "intermediate" region between $2M_W$ and $M_{Z'}$, where deviations from the SM and their increase with energy are directly related to the small shifts in the Z couplings induced by Z-Z' mixing. This is the off-resonance case presented in the next section. In fact, enhanced sensitivity to Z-Z' mixing is also found for $\sqrt{s}$ around $M_{Z'}$, related to the interference and resonance patterns of the cross section, as discussed in Sec. IV. Finally, if the extended model is a renormalizable gauge theory, for $\sqrt{s}\gg M_{Z'}$ (asymptotic region), with all sources of new physics switched on, the gauge cancellation should lead to a decreasing $\ln s/s$ behavior of the cross section. Thus, in general, the enhancement should

occur in the energy region where gauge cancellations are not complete, and for the cases considered here this region extends from $2M_W$ up to about $M_{Z'}$ or even to larger values, provided these are below the asymptotic region.

We should remark that, in principle, we can envisage a more general situation where, in addition to A_Z, the other amplitudes of Fig. 2(a) also have small departures from the SM, so that in Eq. (3) Z would be replaced by either γ and/or ν. By repeating the same procedure, we would easily obtain relations quite similar to Eqs. (6) and (7), only the structure would be more complex since in this case all R_{ij} are involved. The additional deviations from the SM, Δ_γ, and Δ_ν, similarly increase with energy by the mechanism described above. In this case, the relative weights of the different effects can be assessed within specific classes of extended models.

Turning to process (1), one can derive expressions identical to Eqs. (5)–(8) (of course, dropping A_ν), except that in this case of fermion-antifermion final states the functions $R_{ij}^{(f\bar{f})}$ asymptotically tend to a constant with energy. Correspondingly, the statistical uncertainty on cross sections increases with energy at fixed $L_{\rm int}$, while $\Delta_Z^{(f\bar{f})}$ remains constant, so that the sensitivity decreases, in contrast to process (2).

III. OFF-RESONANCE SEARCHES

We start this discussion by assuming for definiteness that at the 95% C.L. level, no signal of Z' is seen for e^+e^- energy up to, e.g., $\sqrt{s}=1$ TeV. We choose this value because it covers current lower limits on the Z' mass. Concerning luminosity, we shall make reference to that anticipated for the Cornell TeV Energy Superconducting Linear Accelerator (TESLA) or NLC, of about 10^{34} cm^{-2}s^{-1}. Also, we assume that the W^+W^- final state is identified via decays into leptons and hadronic jets ($l\nu+jj$).

The direct contribution of the new heavy neutral gauge boson to the amplitude of process (2) is represented by the third diagram in Fig. 2(b). In addition, there are indirect contributions to the Z_1-mediated diagram, represented by modifications of the electronic and three-boson vertices induced by Z-Z' mixing. We define

$$\begin{aligned} Z_1 &= Z\cos\phi + Z'\sin\phi \ , \\ Z_2 &= -Z\sin\phi + Z'\cos\phi \ , \end{aligned} \tag{10}$$

where Z_1 and Z_2 are the physical mass eigenstates, Z and Z' are, respectively, the weak gauge boson eigenstates of SU(2)×U(1) and of the extra U(1)′, and ϕ is the mixing angle:

$$\tan^2\phi = \frac{M_Z^2 - M_1^2}{M_2^2 - M_Z^2} \ , \tag{11}$$

with M_Z the Z mass in the SM

$$(M_Z^2 = M_W^2/\cos^2\theta_W) \ .$$

We shall consider in this section the configuration $M_1 \ll \sqrt{s} \ll M_2$. To a good approximation, for M_2 much larger than M_1, in specific "minimal-Higgs" models [1,7],

$$\phi \simeq -\sin^2\theta_W \frac{\sum_i \langle\Phi_i\rangle^2 I_{3L}^i Q_i'}{\sum_i \langle\Phi_i\rangle^2 (I_{3L}^i)^2} = \mathcal{C}\frac{M_1^2}{M_2^2} \ , \tag{12}$$

where $\langle\Phi_i\rangle$ are the Higgs vacuum expectation values spontaneously breaking the symmetry, and Q_i' are their charges with respect to the additional U(1)′. Thus $\mathcal{C}$ is a model-dependent constant. For example, in the case of E_6 superstring-inspired models $\mathcal{C}$ can be expressed as ($s_W = \sin\theta_W$)

$$\mathcal{C} = 4s_W\left[A - \frac{\sigma-1}{\sigma+1}B\right] \ , \tag{13}$$

where σ is a ratio of vacuum expectation values squared [7], and the constants A and B are reported in Appendix B for the cases of interest here.

The right- and left-handed fermion couplings to Z_1 and Z_2 can be written in general as

$$\begin{aligned} \lambda_1 &= \lambda\cos\phi + \lambda'\sin\phi \ , \\ \lambda_2 &= -\lambda\sin\phi + \lambda'\cos\phi \ , \end{aligned} \tag{14}$$

where

$$\lambda = g_L^f, g_R^f, \quad \lambda' = g_L^{f'}, g_R^{f'} \ . \tag{15}$$

Explicit expressions for λ and λ' in the various models are easily derived from the formulas listed in Appendix B. The ($W^+W^-Z_{1,2}$) couplings can be expressed in terms of the SM coupling $g_{WWZ} = e/\tan\theta_W$ as

$$g_{WWZ_1} = \cos\phi\, g_{WWZ}, \quad g_{WWZ_2} = -\sin\phi\, g_{WWZ} \ . \tag{16}$$

We write the generalization of Eq. (4) for the observable deviation of cross sections from the SM as

$$\Delta_Z(z_1,z_2) = \frac{\sigma(z_1,z_2) - \sigma(z_1,z_2)^{\rm SM}}{\sigma(z_1,z_2)^{\rm SM}} \ , \tag{17}$$

where

$$\sigma(z_1,z_2) = \int_{z_1}^{z_2} \frac{d\sigma}{dz}dz \ , \tag{18}$$

and $z=\cos\theta$. The general formulas to calculate $\sigma(z_1,z_2)$ and $\sigma(z_1,z_2)^{\rm SM}$ for any initial-state polarizations, as well as for unpolarized beams, are reported in Appendix A.

To make the connection with Eq. (3) and the ones which follow, we can consider the full amplitude in Fig. 2 in the approximation of retaining only terms linear in the small mixing angle ϕ and in the mass difference $\Delta M = M_Z - M_1$. This is, in general, a good approximation in the off-resonance energy regime of relevance to this section. Current limits on ϕ and ΔM are, respectively, $|\phi| < 0.02$ and $0 < \Delta M < 340$ MeV [5–8]. With respect to Eqs. (6) and (7) we also have to account for the direct, Z_2-mediated contribution to the relevant interference terms in the cross sections, so that the complete structure

of Δ_Z in (17) is actually (with z_1 and z_2 implicit in the notation)

$$\Delta_Z^{\text{off}}=\Delta_{1Z}+\Delta_{2Z}+\Delta_{3Z}^{\text{interf}} , \tag{19}$$

where Δ_{1Z} and Δ_{2Z} are the same as defined in Eqs. (6) and (7) and $\Delta_{3Z}^{\text{interf}}$ represents the additional direct Z_2 diagram interfering with γ, ν, and Z_1 exchanges.

One can easily derive

$$\epsilon_Z^0=-\frac{2M_Z\Delta M}{s-M_Z^2}=-1.8\times10^{-4}\left[\frac{\Delta M}{\text{GeV}}\right] , \tag{20}$$

for both the polarized (LR or RL e^-e^+ initial states) and the unpolarized cases, while [in the notation of Eq. (15)]

$$\epsilon_{\gamma Z}^{LR}=\epsilon_{\nu Z}^{LR}=\epsilon_{ZZ}^{LR}=\frac{g_L^{e\prime}}{g_L^e}\phi , \tag{21}$$

$$\epsilon_{\gamma Z}^{RL}=\epsilon_{ZZ}^{RL}=\frac{g_R^{e\prime}}{g_R^e}\phi,\quad \epsilon_{\nu L}^{RL}=0 , \tag{22}$$

$$\epsilon_{\gamma Z}^{\text{unpol}}=\frac{v_e'}{v_e}\phi,\quad \epsilon_{\nu Z}^{\text{unpol}}=\frac{v_e'+a_e'}{v_e+a_e}\phi ,$$
$$\epsilon_{ZZ}^{\text{unpol}}=\frac{v_ev_e'+a_ea_e'}{v_e^2+a_e^2}\phi , \tag{23}$$

$$\Delta_{3Z}^{\text{interf}}=-\frac{\text{Re}\chi_2}{\text{Re}\chi_Z}\Delta_{2Z} . \tag{24}$$

In these equations we introduced the vector and axial-vector couplings $v_f,a_f=(g_L^f\pm g_R^f)/2$ and χ's are propagators, i.e.,

$$\chi_Z(s)=s/(s-M_Z^2+iM_Z\Gamma_Z) .$$

The numerical analysis can be easily performed by introducing these expressions into Eqs. (6), (7), and (19), and using the formulas for the SM cross sections, which can be derived from those given in Appendix A. Our results below correspond to an integrated luminosity $L_{\text{int}}=100$ fb^{-1} at 1 TeV. Similar to the findings of Ref. [9], the optimal angular regions where the deviation (19) from the SM is the largest, turn out to be the range $-1\le z\le 0.25$ for $\Delta_Z(z_1,z_2)^{LR}$ and $\Delta_Z(z_1,z_2)^{\text{unpol}}$, and the full angular range for $\Delta_Z(z_1,z_2)^{RL}$. In those ranges, SM integrated cross sections for process (2) are, respectively, $\sigma_{LR}^{\text{SM}}\simeq 310$ fb, $\sigma_{RL}^{\text{SM}}\simeq 20$ fb, and $\sigma_{\text{unpol}}^{\text{SM}}\simeq\frac{1}{4}\sigma_{LR}^{\text{SM}}$. Using the channel of leptons plus two hadronic jets to identify the final W^+W^- state, one obtains the 2σ statistical uncertainties of about 2%, 8%, and 4%, respectively. To obtain bounds on the mixing angle ϕ we demand that, for a positive signal, Δ_Z in Eq. (17) should be greater than the 2σ uncertainty on cross sections, which means that our limits will be at 95% C.L. Using (19) and (11) for fixed ΔM and at a given level of statistical accuracy, one can easily assess the typical upper bounds on ϕ which can be reached by this kind of analysis for the various models. These bounds turn out to be of the order of 10^{-4}.

In Figs. 4(a) and 4(b) we depict the best upper limits on ϕ, respectively for effective E_6 models [classified by the values of β, which specifies the orientation of the additional U(1)′ generator in the E_6 group space], and for both the LRM (specified by α_{LR} defined in Appendix B) and the ALRM. For each curve in Figs. 4(a) and 4(b) the labels a and b specify which case (initial RL or LR beams polarizations) gives the best limits for the corresponding part of the curve. The curves in these figures (as well as in all figures in the sequel), are obtained by using the precise formulas for the cross sections presented in Appendix A. In the case of the LRM we have assumed that mixing in the charged sector is negligible with respect to mixing in the neutral sector [7]. The results in Figs. 4(a) and 4(b) weakly depend on the chosen value of ΔM (within the assumed present limits), because Δ_{2Z} is found to numerically dominate in Eq. (19) for any choice. In contrast, the corresponding lower bounds on the heavy boson mass M_2, as obtained through Eq. (11), significantly depend on the chosen value of ΔM. We

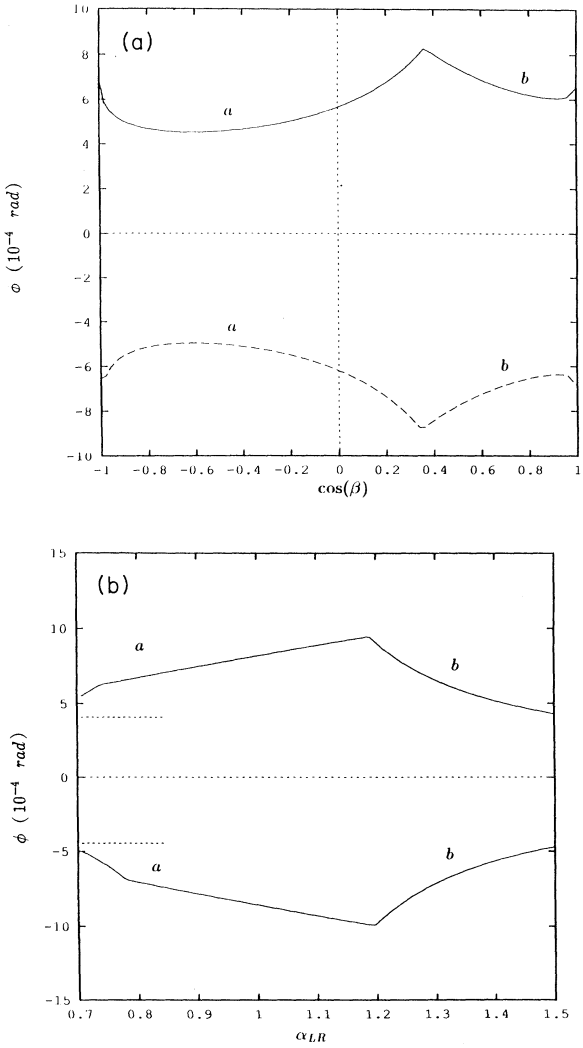

FIG. 4. (a) 95% C.L. limits on ϕ for E_6 effective models vs $\cos\beta$ from $e^+e^-\to W^+W^-$ at $\sqrt{s}=1$ TeV, $\Delta M=50$ MeV; a from the RL polarization and b from the LR polarization, as explained in the text (Sec. III). (b) Same as in (a), for LRM (solid line) and ALRM (dotted).

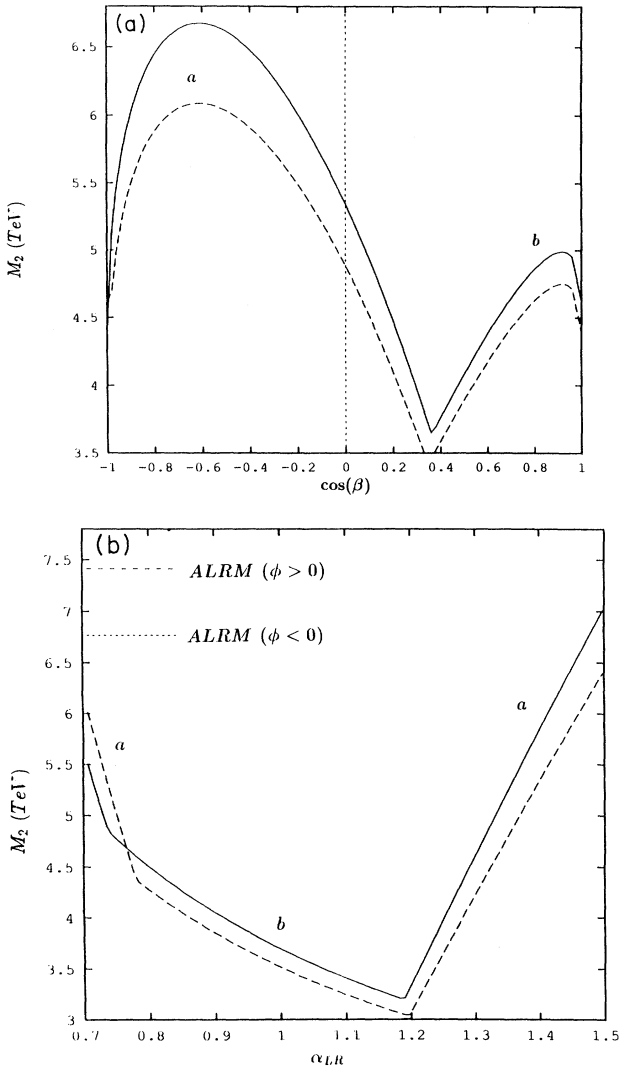

FIG. 5. (a) 95% C.L. limits on the Z_2 mass corresponding to Fig. 4(a) for $\phi > 0$ (solid line) and $\phi < 0$ (dashed line); a and b as in Fig. 4(a). (b) Same as in (a), for LRM and ALRM.

represent in Figs. 5(a) and 5(b) the bounds on M_2 for the models mentioned above, for $\Delta M = 50$ MeV.[1] For the upper limit $\Delta M = 340$ MeV, the bounds in Figs. 5(a) and 5(b) are improved by a factor of the order of 2.5.

It might be interesting to restrict the E_6 models to a class of models where the Higgs structure is specified, so that the constant $\mathcal{C}$ in Eq. (13) is fixed and relates the mixing angle ϕ to the heavy boson mass Z_2 through Eq. (12) [7]. Using the relevant formulas for the coupling constants given in Appendix B we obtain the results represented in Fig. 6.

[1]This value corresponds to the 90% C.L. lower bound at $m_t = m_H = 100$ GeV and $\alpha_s = 0.12$, as found in Ref. [5].

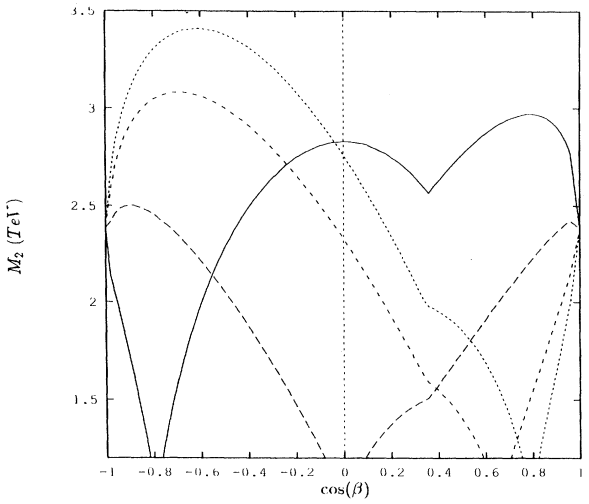

FIG. 6. 95% C.L. limits on the Z_2 mass from $e^+e^- \to W^+W^-$ in E_6 superstring-motivated models for different values of the parameter σ introduced in Eq. (13): $\sigma = 0$ (solid line), $\sigma = 1$ (long-dashed line), $\sigma = 5$ (short-dashed line), and $\sigma = \infty$ (dotted line).

IV. ON- AND NEAR-RESONANCE SEARCHES

To discuss this case, we assume that the Z_2 resonance is observed through process (1) at, for example, $\sqrt{s} = M_2 = 1$ or 2 TeV, so that from precision measurements at the Z_2 peak the fermionic couplings and the Z_2 mass could be extracted with some accuracy. We also assume in this section and in the next Sec. V that the energy spread of initial beams is smaller than the total Z_2 width.

The accuracy on the peak $f\bar{f}$ cross section could be such as to allow, within definite models, to also derive indications or bounds on the value of the mixing angle ϕ, as it was traditionally done at the standard Z. Of course, with a given precision, this possibility depends on the actual value of ϕ and might not exist for ϕ smaller than allowed by the accuracy. As we are going to show below, in this situation it should be convenient to study process (2) at the resonance Z_2. In fact, for these values of ϕ one could still have an effect of mixing in process (2) larger than (or comparable to) the accuracy available for this channel, or at least some constraints could be derived.

In this on-resonance case, Eq. (19) must be modified to

$$\Delta_Z = \Delta_Z^{\text{off}} + \Delta_{3Z}^{\text{res}} \tag{25}$$

in order to take into account the leading ϕ^2 contribution from Z_2 exchange, with Δ_Z^{off} as defined in (17) but evaluated at $\sqrt{s} = M_2$. Specifically,

$$\Delta_{3Z}^{\text{res}} \cong \left[\frac{\lambda'}{\lambda}\right]^2 R_{ZZ} \left|\frac{\chi_2}{\chi_Z}\right|^2 \phi^2 , \tag{26}$$

with λ, λ' defined in Eq. (15) and R_{ZZ} in Eq. (8). The propagators χ_2 and χ_Z have been previously introduced with regard to Eq. (24).

The strong energy behavior of R_{ZZ} (and of the ratio

χ_2/χ_Z) in (26) leads to the enhancement of the sensitivity to ϕ of the cross sections at the resonance peak. Indeed, Eq. (25) contains both linear terms in ϕ (from $\Delta_Z^{\rm off}$) and quadratic ones [from $\Delta_{3Z}^{\rm res}$ as well as from $\Delta_Z^{\rm off}$ expanded to a higher order than in Eqs. (21)–(24)]. One can easily see that in (19) $\Delta_{3Z}^{\rm interf}=0$ at $\sqrt{s}=M_2$. At the energy considered here, $\Delta_{3Z}^{\rm res}$ is found to numerically compete with the linear terms for ϕ of the order of magnitude corresponding to the assumed accuracy, while the quadratic terms contributed by $\Delta_Z^{\rm off}$ are negligible both compared to the linear ones and to $\Delta_{3Z}^{\rm res}$, so that to a very good approximation they can be disregarded in the analysis.

Regarding the ratio of propagators in (26), at the Z_2 peak,

$$\left|\frac{\chi_2}{\chi_Z}\right|^2 \cong \left[\frac{M_2}{\Gamma_2}\right]^2 , \tag{27}$$

so that there is a significant dependence on the Z_2 total width Γ_2, which should also be measured together with M_2 in process (1), but for the moment we assume to be unknown. For our purposes we identify

$$\Gamma_2=\sum_f \Gamma_2^{ff}+\Gamma_2^{WW} . \tag{28}$$

Further contributions of decays involving Higgs and/or gauge bosons and the supersymmetric partners (including sfermions), which are not accounted in (28), could increase Γ_2 by a model-dependent amount typically as large as 50% [1].

$\sum_f \Gamma_2^{ff}$ depends on the number n_g of generations of heavy exotic fermions which can contribute to Z_2 decay without phase space suppression (we can assume that the three known generations do contribute). This number is model dependent too, and brings a phenomenological uncertainty. For E_6 models, the extreme cases are $n_g=0$ and $n_g=3$ [20]. From the point of view of constraining the mixing angle ϕ [see Eqs. (26) and (27)], the most conservative choice would be $n_g=3$, leading to larger Γ_2, of the order of $\sum_f \Gamma_2^{ff}\simeq 0.025 M_2$ [20], independent of both $\cos\beta$ and (in the linear approximation) of ϕ. More stringent limits would be obtained for $n_g=0$, leading to smaller $\sum_f \Gamma_2^{ff}$, by a factor 2–5. For the range of M_2 values assumed here, of the order of 1 or 2 TeV, the dependence of Γ_2 on ϕ (and on $\cos\beta$) induced by $\sum_f \Gamma_2^{ff}$ and by Γ_2^{WW} is unimportant in Eq. (26), which refers to W^+W^- production at the Z_2 peak and therefore is already of order ϕ^2.[2] Using Eqs. (25) and (11) for fixed M_2 (and given accuracy) one can easily derive a qualitative estimate of the limitations on ϕ, which turn out to be of the order of 10^{-5}–10^{-4}.

We present the bounds on ϕ for both cases $n_g=0$ and $n_g=3$ in Fig. 7(a) for $M_2=1$ TeV, while the dependence of such bounds on the different values of M_2 is shown in Fig. 8 (limiting to $n_g=3$). The comparison of Figs. 4(a) and 7(a) shows that the on-resonance analysis can lead to a gain of a factor as large as 5, compared to the off-resonance one.

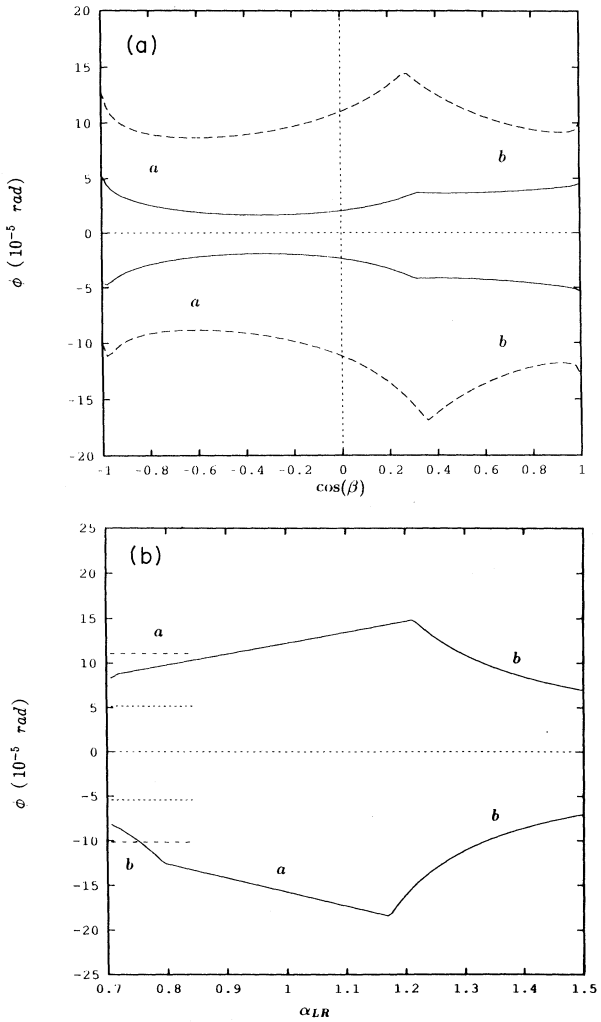

FIG. 7. (a) 95% C.L. limits on ϕ for effective E_6 models vs $\cos\beta$ from $e^+e^-\to W^+W^-$ at $\sqrt{s}=M_2=1$ TeV, for $n_g=0$ (solid line) and $n_g=3$ (dashed line); a and b as in Fig. 4(a). (b) Same as (a) for LRM (solid line) and ALRM: $n_g=3$ (dashed line), $n_g=0$ (dotted line).

Concerning the other models (LRM or ALRM), the discussion of Γ_2 is not as systematic: basically, in the LRM we can still assume to a good approximation the value of $\sum_f \Gamma_2^{ff}$ corresponding to the case $n_g=3$ for E_6 models (regardless of whether the right-handed neutrino is light or heavy), while for the ALRM the extreme values of $\sum_f \Gamma_2^{ff}$ are $(0.02$–$0.04)M_2$ for $n_g=0$ and $n_g=3$, respectively [15,21]. The constraints for ϕ in these models are shown in Fig. 7(b), which again, analogously to Fig. 7(a), shows the better sensitivity of the on-resonance analysis.

We now turn to the near-resonance searches, specifically to the cross-section measurements at

$$\sqrt{s}=M_2\pm\Gamma_2/2 . \tag{29}$$

[2]In contrast, this dependence can have an important role in $f\bar{f}$ production, as it will be discussed in Sec. V.

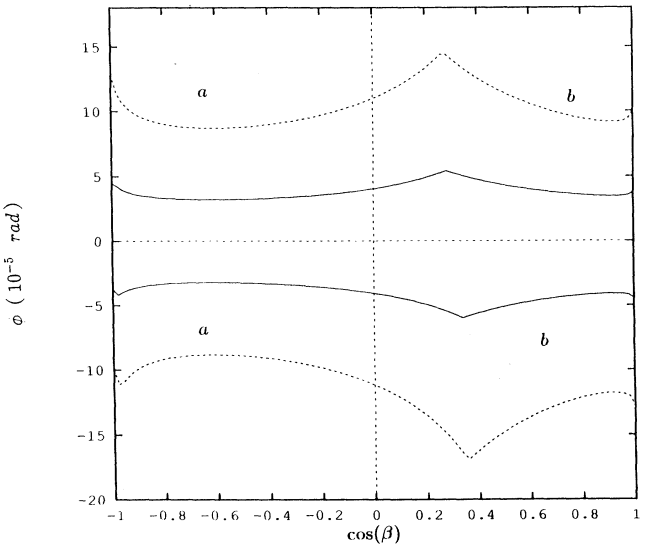

FIG. 8. Same as in Fig. 7(a), but for $M_2=1$ TeV (dotted line) and $M_2=2$ TeV (solid line): $n_g=3$.

At this value of the energy the cross section of process (2) has contributions of order ϕ from the Z_2-interference terms, and of order ϕ^2 from the Z_2-exchange diagram squared. For small enough ϕ the former terms can become numerically comparable (or even larger) than the latter one. We present this situation for the different values of ϕ in Fig. 9, which shows that the resonance peak, for decreasing ϕ, turns into a typical interference pattern, and eventually disappears with respect to the near-resonance cross section. Thus, for such small values of ϕ, one could hope to obtain a further increased sensitivity to the mixing angle from the near-resonance cross section (as compared to the on-resonance one) and accordingly it would be quite interesting to scan the energy

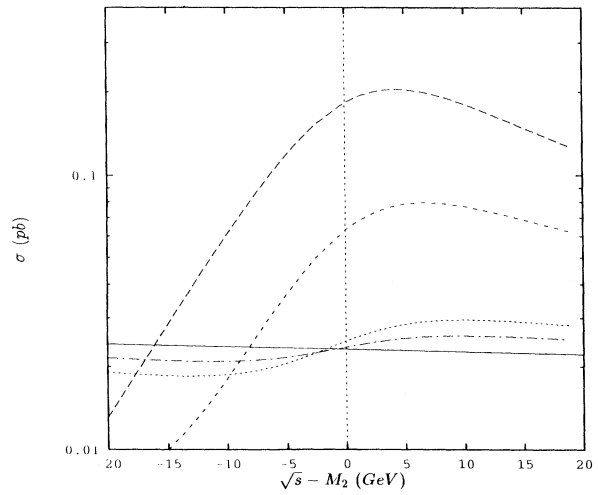

FIG. 9. Near-Z_2 resonance total cross section for the ψ model, $M_2=1$ TeV for RL polarization. SM (solid line), $\phi=10^{-3}$ (long-dashed line), $\phi=5\times10^{-4}$ (short-dashed line), $\phi=10^{-4}$ (dotted line) and $\phi=5\times10^{-5}$ (dash-dotted line).

range in the vicinity of the resonance peak. As it can be seen from Eq. (25), the corresponding improvement on the limitations on ϕ can be expressed by the factor

$$\left|\frac{\phi^{\text{off}}}{\phi^{\text{near}}}\right|=\left|\frac{\text{Re}\chi_2}{\text{Re}\chi_Z}\right|\approx\frac{M_2}{2\Gamma_2}=20-100\ , \tag{30}$$

where the smaller value corresponds to $n_g=3$ and the larger one to $n_g=0$. Figure 10(a) shows the limits on the mixing angle obtained at the energy (29) for $n_g=0$ and $n_g=3$. For the other models the limits are displayed in Fig. 10(b).

V. COMPARISON WITH $e^+e^-\to f\bar{f}$

In this case there are numerous available channels to look at (leptonic and hadronic, either inclusive or exclusive, final states) as well as many observables to measure, such as the total unpolarized and polarized cross sections, their ratios, forward-backward leptonic asymmetries and left-right asymmetries for both leptonic and

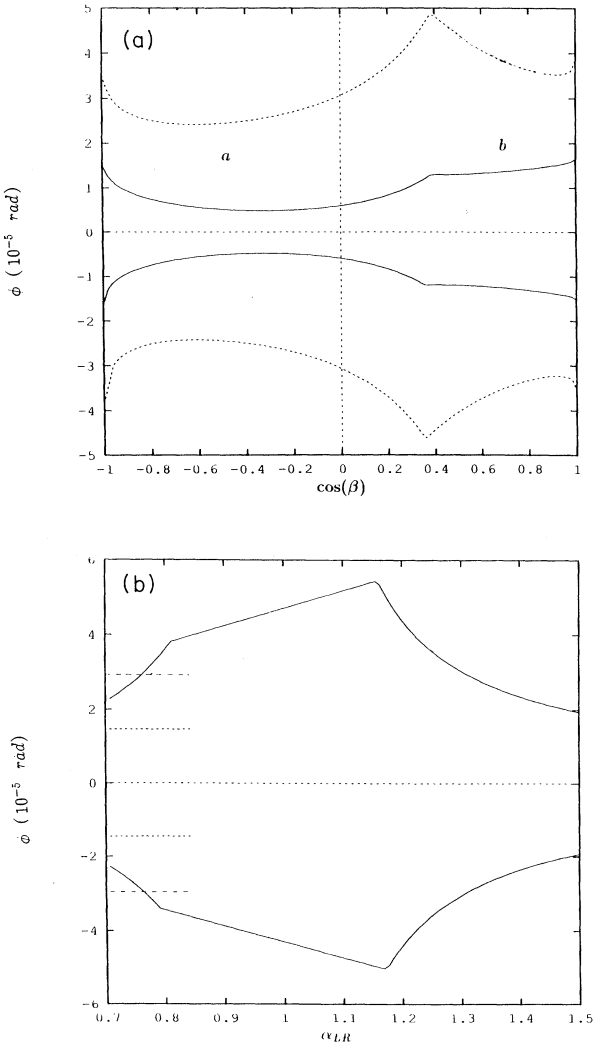

FIG. 10. (a) Same as in Fig. 7(a), but $\sqrt{s}=M_2\pm\Gamma_2/2$. (b) Same as in Fig. 7(b), but $\sqrt{s}=M_2\pm\Gamma_2/2$.

hadronic final states, etc. Because of the large peak cross sections, the common expectation is that it should be possible to derive from this process great accuracies on the fermionic couplings of the Z_2 and possibly stringent bounds on the mixing angle. This kind of analysis is being carried out at the standard Z peak, and should be repeated equally well at the Z_2, with the same physical outcomes. However, as anticipated in the previous section, concerning the determination of the Z' properties and, in particular, of Z-Z' mixing, the process $e^+e^-\to W^+W^-$ could be sensitive to values of ϕ out of reach for $e^+e^-\to f\bar{f}$, due to the enhancement mechanism discussed in Secs. II and III, and extended to the on- and near-resonance cases in Sec. IV.

Since in the off-resonance energy regime the cross section of process (1) is too small for the accuracy needed to improve current limits on Z-Z' mixing, we compare the two processes for just the case of on-resonance searches. Specifically, at $\sqrt{s}=M_2$, the most relevant observables for process (1) are

$$\begin{aligned}
&\sigma_{\mu\mu}\equiv\sigma(e^+e^-\to\mu\bar{\mu})=\frac{12\pi}{M_2^2}\left[\frac{\Gamma_2^{\mu\mu}}{\Gamma_2}\right]^2,\\
&R'\equiv\frac{\sigma(e^+e^-\to u,d,s,c,b)}{\sigma_{\mu\mu}}=\frac{\Gamma_2^h}{\Gamma_2^{\mu\mu}},\\
&A_{FB}^{\mu}=3(A_\mu)^2,\\
&A_{LR}^{\mu,h}=-2A_\mu,
\end{aligned}\tag{31}$$

where, in terms of the Z_2 fermionic couplings,

$$A_f=\frac{v_{2f}a_{2f}}{v_{2f}^2+a_{2f}^2}\tag{32}$$

and, referring to Eq. (14), $v_{2e}=(g_{2L}^e+g_{2R}^e)/2$ and $a_{2e}=(g_{2L}^e-g_{2R}^e)/2$. Clearly, in Eq. (31) $\sigma_{\mu\mu}$ has an n_g dependence through the total width Γ_2, similarly to (27), whereas the observables R', A_{FB}^{μ}, and $A_{LR}^{\mu,h}$ do not have such a dependence. However, in all cases the expected statistical accuracy will depend on Γ_2 via the dependence of the Z_2-peak cross sections of process (1) on n_g, so that also in this case bounds on ϕ will have this model dependence. Denoting by F any of the observables (31), in the presence of Z-Z' mixing one generally has

$$F\simeq F(0)(1+H_F\phi),\tag{33}$$

where $F(0)=F(\phi=0)$ is the value of the observable in the absence of mixing, and H_F is a specific coefficient for each observable, explicitly given in Appendix C in terms of the relevant Z_2 fermionic coupling constants. Comparing with Eq. (17), the quantity $\Delta_Z^{ff}=H_F\phi$ is the analogous of Δ_Z for process (2), and as such it has to be compared to the relative experimental accuracy on the cross sections of process (1) in order to obtain limits on ϕ. As an example, the values H_F for E_6 models are reported in Fig. 11. One finds that, by explicitly computing cross sections in the framework of these models, the expected statistical accuracies for all observables [13] can be of the order of 0.5% for $n_g=3$ and even less for $n_g=0$, much better than those expected for process (2). From Eq. (33)

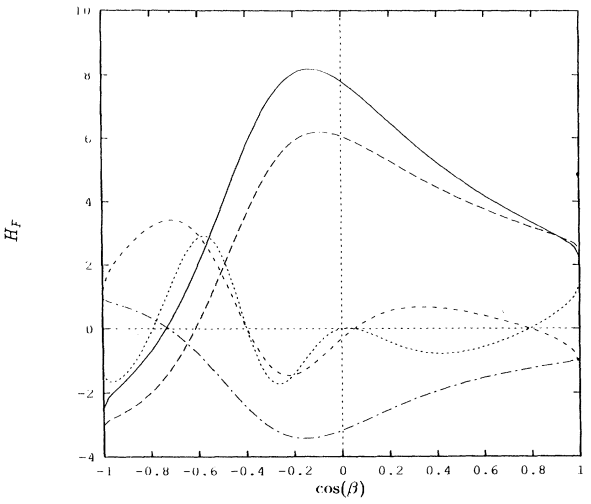

FIG. 11. H_F of Eq. (33) vs cosβ. H_σ for $n_g=3$ (solid line), H_σ for $n_g=0$, (long-dashed line), H_{LR} (short-dashed line), H_{FB} (dotted line) and $H_{R'}$ (dash-dotted line).

and the curves in Fig. 11 one can conclude that the most stringent bounds on the mixing angle ϕ come from the observables $\sigma_{\mu\mu}$ and A_{LR}^h (statistics are larger for the inclusive hadronic channel), in complementary ranges of cosβ. These bounds are shown in Fig. 12, for the (most favorable) case $n_g=0$, and for $M_2=1$ TeV. For larger values of M_2 the expected limits are found to become weaker for all observables, because statistics will decrease due to the fall-down of the peak cross sections in the various models, except for $\sigma_{\mu\mu}$. In Fig. 12 we represent also the expected bounds on ϕ for $M_2=2$ TeV and $M_2=3$ TeV. While at $M_2=1$ TeV the bounds for the different values of cosβ are determined by the combined set of observables (31), as explicitly indicated in Fig. 12, for larger

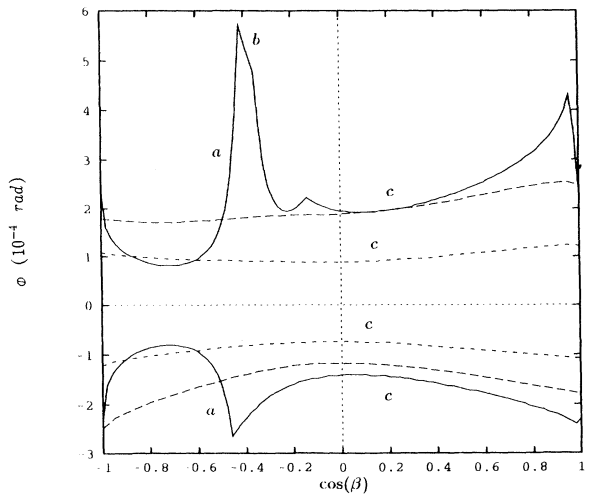

FIG. 12. Limits on the mixing angle ϕ in E_6 effective models from $e^+e^-\to f\bar{f}$, for the on-Z_2 resonance case ($n_g=0$), at $M_2=1$ TeV (solid line), $M_2=2$ TeV (long-dashed line) and $M_2=3$ TeV (short-dashed line). (a) from A_{LR}^h, (b) from R', and (c) from $\sigma_{\mu\mu}$.

M_2 they are determined by $\sigma_{\mu\mu}$ solely. This reflects the fact that for large M_2 the contribution of Γ_2^{WW} to the total width Γ_2 in Eq. (C18), although of order ϕ^2, becomes competitive with the linear term in (33) and overwhelms it, due to the M_2^4 behavior of Eq. (C17) relative to (C4). This contribution of Z-Z' mixing to $\sigma_{\mu\mu}$ at the peak $\sqrt{s}=M_2$ increases faster than the decrease in the statistical accuracy caused by the $1/M_2^2$ falloff of the cross section of process (1), and compensates it.

Comparing to process (2), where also the cross sections and the corresponding statistics fall down, but deviations from the SM [Eq. (25)] grow faster due to the increasing behavior of R_{ZZ}, Figs. 8 and 12 indicate that the behavior of the constraints on ϕ as a function of M_2 from this process is qualitatively similar to the $f\bar{f}$ case, although having a different origin.

Concerning the sensitivities of the two processes to the mixing angle ϕ, it should be worth emphasizing the essential conceptual difference between the two kinds of approaches to the problem. Indeed, while the bounds on ϕ from $e^+e^-\to f\bar{f}$ come from the supposed observation of the Z_2 resonance peak, those from $e^+e^-\to W^+W^-$ are derived by assuming the nonobservation of deviations from the SM cross section larger than the expected statistical accuracy. From the numerical point of view, the values of bounds from the two processes can be compared by looking at Fig. 12 and Figs. 7(a) and 10(a). These figures show that the sensitivity of process (2) to the mixing angle is much higher, by roughly one order of magnitude. This can be qualitatively understood by considering that the sensitivity of process (1) to ϕ is basically

$$\phi_{ff}\approx\frac{\delta\sigma_{ff}/\sigma_{ff}}{H_F} \tag{34}$$

in the linear approximation (33). In turn, in the near-resonance case the sensitivity to ϕ of process (2), following from the solution of Eq. (25), can be represented as

$$\phi_{WW}\approx\frac{\delta\sigma_{WW}/\sigma_{WW}}{H_W} \tag{35}$$

where, for the example, for the LR case,

$$H_W^{LR}=-\frac{g_L^{e'}}{g_L^e}\frac{\mathrm{Re}\chi_2}{\mathrm{Re}\chi_Z}(R_{\gamma Z}+R_{\nu Z}+2R_{ZZ})\ , \tag{36}$$

and a similar structure is simply obtained for the RL and the unpolarized cases. The point now is that numerically H_W turns out to be $\sim 3\times(10^2-10^3)H_F$, and to largely compensate the difference in statistical accuracies between the two processes due to the different cross sections.

VI. CONCLUDING REMARKS

In this section we summarize the most important features of the method to study Z-Z' mixing described above, and make some general statements on the corresponding results presented in Figs. 4–10. In the approach proposed here, information on Z-Z' mixing and corresponding limits on the Z' mass in various kinds of extended models are obtained through studies of the process $e^+e^-\to W^+W^-$ in the energy range available at planned e^+e^- supercolliders. Also, we have made comparisons with the sensitivity to mixing obtainable from the reaction $e^+e^-\to f\bar{f}$, for different hypothetical values of the Z' mass, larger or equal to 1 TeV as compatible with the present limits. The results for this case are illustrated in Fig. 12.

Starting from process (1), this turns out to be most useful just at the Z_2-resonance peak (if this is discovered), and the information on mixing would be derived from precise measurements of $Z_2 f\bar{f}$ couplings via Eq. (14), similar to present analyses at the SM Z peak, and possibly improving them. For the lower values of Z_2 masses in the considered range (1–3 TeV), the most stringent limits on ϕ are determined by combining the various observables (31). For the larger values of M_2 the limits can become more stringent, but are determined by $\sigma_{\mu\mu}$ only. As pointed out in the previous section, this feature is connected to the increasing contribution of the partial width Γ_2^{WW} to the total width Γ_2. Numerically, the typical bounds on the mixing angle ϕ are *a few* $\times 10^{-4}$ rad. Out of the resonance peak the limits evidently become much worse, due to the sharp decrease of the statistical accuracy.

Concerning $e^+e^-\to W^+W^-$ [process (2)], Z-Z' mixing is studied in this case by looking at deviations of measured cross sections from SM predictions as defined in Eq. (17), relative to the experimental uncertainty on cross sections. We recall that in process (2) Z' effects only occur via mixing, and therefore are of order ϕ or ϕ^2 depending on the explored mass and energy regions, whereas in process (1) the Z' can manifest itself mostly via the direct Z_2 propagator and Z-Z' mixing would only appear as a (small) deviation at the Z_2 peak. Therefore, the two kinds of approach to search for manifestations of Z-Z' mixing at e^+e^- colliders are intrinsically different. As another difference, the available statistical accuracy for $e^+e^-\to W^+W^-$ is identified to that expected from the SM, and would clearly be much smaller than for $e^+e^-\to f\bar{f}$ at the Z_2 peak, because for small values of ϕ the Z_2 might not manifest as a peak in W^+W^- while there would certainly be a peak in $f\bar{f}$ independent of the smallness of ϕ.

Nevertheless, our results indicate that the expected limits on the mixing angle ϕ from process (2), even off the Z_2 resonance peak ($\sqrt{s}\ll M_2$), are comparable with the on-resonance ones from process (1), due to the enhancement mechanism presented in Sec. II, and therefore measurements of the cross sections of process (2) would be quite significant in the case where the Z_2 could not be directly observed. Moreover, if the energy of e^+e^- beams allows to reach the Z_2 peak, on-resonance measurements of the cross section of process (2) would lead to much more stringent constraints on ϕ, typically of the order of *a few* $\times 10^{-5}$–*a few* $\times 10^{-4}$ depending on models ($n_g=0$ or 3). These limits would be a factor 5–10 better than those from reaction (1) for the same values of n_g. Further improvements could be derived from near-resonance measurements at $\sqrt{s}=M_2\pm\Gamma_2/2$. For example, the near-resonance limits on ϕ might be stronger

than the off-resonance ones by a factor of 20–100, also depending on n_g, and as small as 10^{-6}–10^{-5}. In general, these constraints improve for increasing values of M_2.

Turning to lower bounds on the Z_2 mass, obtained from the off-resonance analysis of process (2) in Sec. III, for E_6 effective models they are in the range 3–6 TeV for the choice $\Delta M = 50$ MeV. The other choice, corresponding to the presently allowed upper value $\Delta M = 340$ MeV, leads to mass bounds higher by a factor of about 2.5. Regarding other models (ALRM or LRM) slightly stronger limits can be obtained, while for superstring-motivated E_6 models the bounds are as large as 3.5 TeV.

Another important aspect to be emphasized is the role, in establishing limits on Z-Z' mixing from W^+W^-, played by polarized cross sections: typically, limits from the LR cross section are by a factor of 2 more stringent than those from the unpolarized one [9], assuming that e^+e^- polarization near 100% is feasible. In contrast, in the case of $f\bar{f}$ production the best limits mostly come from the unpolarized cross section ($\sigma_{\mu\mu}$), especially for the larger values of M_2.

Clearly, the numerical results presented in the previous sections are based on purely statistical arguments. However, it is natural to assume that systematic experimental uncertainties at future colliders should be comparable to the statistical ones, determined by the luminosities, so that we may be confident that the scenario presented in Secs. III–V should be sufficiently close to reality, particularly for what concerns the comparison of the relative features of processes (1) and (2). Moreover, we used throughout the Born approximation for the relevant cross sections of both processes. Thus, admittedly it should be desirable to account also for radiative corrections, which could shift the values of cross sections by some amount and somehow perturb the numerical predictions. However, our findings from process (2) are essentially based on the enhancement mechanism introduced in Sec. II, determined by the energy behaviors of the different contributions to the cross section, which should not be drastically changed by the mentioned higher-order corrections. Therefore, the general ideas underlying the approach presented here should be preserved.

As a final remark, we remind that in the above discussion of process (2) we essentially considered the (extreme) case where no deviation from the SM due to Z' mixing is seen in this process within the experimental accuracy. We accordingly derived maximal values of the Z-Z' mixing angle $|\phi|$, which are well below the value allowed by the general mass constraint (11) at fixed ΔM. We could now take the opposite attitude and consider the other (extreme) situation, where $|\phi|$ assumes the maximum value allowed by (11) for a fixed value of ΔM. Of most interest in this case is the behavior of the total Z_2-peak cross section for increasing M_2, which can be simply expressed by the Breit-Wigner formula

$$\sigma_{WW}(M_2) = \frac{12\pi}{M_2^2}\frac{\Gamma_2^{ee}\Gamma_2^{WW}}{\Gamma_2^2} \ . \tag{37}$$

From Eqs. (C2), (C17), and (11), the leading M_2 behaviors relevant to Eq. (37) are, respectively, $\Gamma_2^{ff} \propto M_2$, $\Gamma_2^{WW} \propto M_2^5\phi^2$, and $\phi \propto 1/M_2$ at fixed ΔM. Referring to Eqs. (28) and (C18), and defining

$$\omega = \frac{\Gamma_2^{WW}}{\sum_f \Gamma_2^{ff}} \ , \tag{38}$$

for the values of M_2 such that $\omega \ll 1$ one easily finds that $\sigma_{WW}(M_2)$ is a *constant*, independent of M_2, as opposed to the $\ln s/s$ decrease of the SM cross section.[3] For larger values of M_2 the ratio ω is no longer negligible, and actually becomes of order 1, due to its behavior $\propto M_2^2$, and must be included in Γ_2. Correspondingly, in this range of M_2 the behavior implied by (37) is the strongly decreasing asymptotic dependence $\sigma_{WW}(M_2) \propto 1/M_2^4$. The transition from the flat behavior to the asymptotic decrease occurs in an energy range which depends both on the particular model and on n_g. These features are represented in Fig. 13, where we show the behavior of ω vs M_2 for $n_g = 3$ and 0, and for two values of ΔM. Finally, in Fig. 14 we depict the cross sections for the different values of M_2 (and for $\Delta M = 50$ MeV), as well as the SM background. For illustrative purposes in Figs. 13 and 14 we have considered the broad range of M_2 from 0.5 TeV up to 15 TeV.

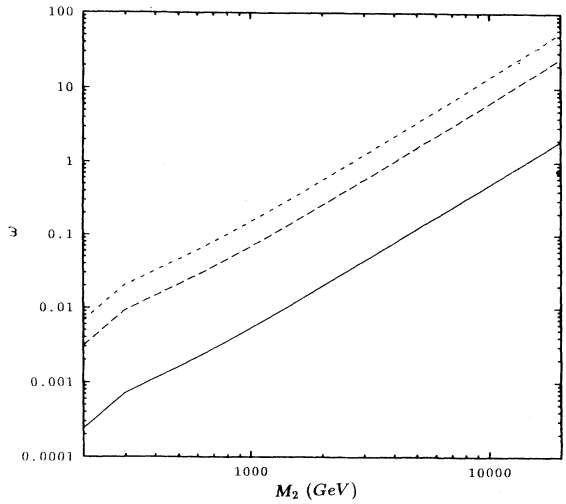

FIG. 13. ω of Eq. (38) as a function of M_2, for $n_g = 3$, $\Delta M = 50$ MeV (solid line) and for $n_g = 0$, $\Delta M = 300$ MeV in the χ model (long-dashed line), and in the ψ model (short-dashed line).

[3]Actually, for specific models where the mixing angle decreases like $1/M_2^2$, such as in Eq. (12), the behavior of $\sigma_{WW}(M_2)$ would be $\propto 1/M_2^2$. However, we are considering here the most general case, where the dependence of ϕ on M_2 is defined via (11).

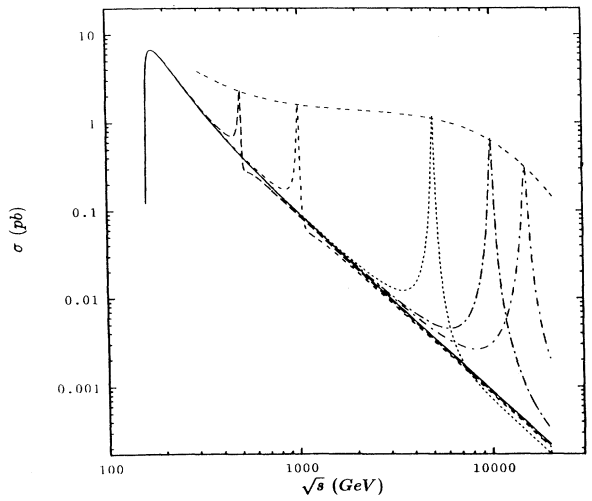

FIG. 14. Total $e^+e^- \to W^+W^-$ cross section vs $\sqrt{s}$ for the χ model with different Z_2 masses, $\Delta M = 50$ MeV, $n_g = 3$. The solid line represents the SM behavior.

It is interesting to observe from Fig. 14 that in the region of flat behavior the height of the peaks relative to the SM background increases, and for larger M_2 might be larger than the SM cross section by a factor 10^2–10^3, which promises enhanced chances of direct observation of the Z_2 if one works at fixed luminosity. On the other hand, this situation does not persist indefinitely, and the decreasing behavior at the higher values of M_2 clearly reduces this discovery potential.

Turning to $f\bar{f}$ production [process (1)], analogous considerations indicate for the Z_2-peak cross sections

$$\sigma_{f\bar{f}}(M_2) \propto 1/M_2^2(1+\omega)^2 ,$$

the same as the SM background behavior $\propto 1/s$ for $\omega \ll 1$. This decrease would become steeper for the larger M_2, where ω is of order 1.

These features of $e^+e^- \to W^+W^-$ production would remain the same also for $q\bar{q} \to W^+W^-$ and, given the large values of M_2 considered in Fig. 14, could be relevant to direct Z_2 searches at future hadron colliders.

ACKNOWLEDGMENTS

One of the authors (A.A.P.) would like to express his gratitude to Professor A.S. Shaginyan for continuing encouragement and help, and to INFN-Sezione di Trieste for financial support. He also thanks Professor Abdus Salam, the International Atomic Energy Agency and UNESCO for hospitality at the International Centre for Theoretical Physics, Trieste. N.P. was supported by MURST.

APPENDIX A

For the process $e^+e^- \to W^+W^-$ the differential cross section can be decomposed as follows:

$$\frac{d\sigma}{dz} = \frac{\pi\alpha_{\rm QED}^2}{16\sin^4\theta_W}\frac{\beta_W}{s}\left[\bar{\sigma}_{\nu\nu}+\bar{\sigma}_{\gamma\gamma}+\bar{\sigma}_{\gamma\nu} + \sum_{i=1,2}(\bar{\sigma}_{\gamma Z_i}+\bar{\sigma}_{\nu Z_i}) + \sum_{i,j=1,2}\bar{\sigma}_{Z_iZ_j}\right] , \tag{A1}$$

where we use the notation $\bar{\sigma} = d\sigma/dz$, $z = \cos\theta$. We have from the diagrams in Fig. 2(b) for initial $e_L^- e_R^+$ (LR):

$$\begin{aligned}
&\bar{\sigma}_{\nu\nu}^{LR} = 4F_1, \quad \bar{\sigma}_{\gamma\gamma}^{LR} = 2s_W^4 F_2, \quad \bar{\sigma}_{\gamma\nu}^{LR} = -4s_W^2 F_3 , \\
&\bar{\sigma}_{\gamma Z_i}^{LR} = -4\frac{g_i^e}{g_1}s_W^2\,{\rm Re}\chi_i F_2, \quad \bar{\sigma}_{\nu Z_i}^{LR} = 4\frac{g_i^e}{g_1}\,{\rm Re}\chi_i F_3 , \\
&\bar{\sigma}_{Z_iZ_i}^{LR} = 2\left[\frac{g_i^e}{g_1}\right]^2|\chi_i|^2 F_2 , \\
&\bar{\sigma}_{Z_1Z_2}^{LR} = \bar{\sigma}_{Z_2Z_1}^{LR} = 2\frac{g_1^e g_2^e}{g_1^2}\,{\rm Re}(\chi_1\chi_2^*)F_2 ,
\end{aligned} \tag{A2}$$

where $\beta_W = (1-4M_W^2/s)^{1/2}$ is the velocity of the W and the χ's are the Z_1 and Z_2 propagators, $\chi(s) = s/(s-M^2+i\Gamma M)$. In Eq. (A2) we have $g_1 = e/s_W c_W$,

$$g_i^e = g_{iL}^e g_{WWZ_i}/g_{WWZ} ,$$

and the functions F are defined as ($y = s/M_W^2$, $x = t/M_W^2$, $t = M_W^2 - s/2 + sz\beta_W/2$):

$$\begin{aligned}
&F_1 = 2y + \frac{1}{2}(1-z^2)\beta_W^2\left[\left[\frac{y}{x}\right]^2 + \frac{1}{4}y^2\right] , \\
&F_2 = \beta_W^2[16y + (y^2-4y+12)(1-z^2)] , \\
&F_3 = 16\left[1+\frac{1}{x}\right] + 8y\beta_W^2 + \frac{1}{2}\left[y^2-2y-4\frac{y}{x}\right]\beta_W^2(1-z^2) .
\end{aligned} \tag{A3}$$

Integrating from z_1 to z_2,

$$\sigma(z_1,z_2) = \int_{z_1}^{z_2}\frac{d\sigma}{dz}dz , \tag{A4}$$

one has a similar structure as in (A2), except that F_1, F_2, F_3 are replaced by

$$\begin{aligned}
&G_1(z_1,z_2) = 2yP_1 + \frac{1}{2}\beta_W^2\left[P_3 + \frac{y^2}{4}P_2\right] , \\
&G_2(z_1,z_2) = \beta_W^2[16yP_1 + (y^2-4y+12)P_2] , \\
&G_3(z_1,z_2) = 16(P_1+P_5) + 8y\beta_W^2 P_1 + \frac{1}{2}[(y^2-2y)P_2 - 4P_4]\beta_W^2 ,
\end{aligned} \tag{A5}$$

with

$$P_1(z_1,z_2)=z_2-z_1,\quad P_2(z_1,z_2)=P_1-\frac{z_2^3-z_1^3}{3},$$

$$P_3(z_1,z_2)=b^2\left[2aL_1+(a^2-1)\left[\frac{1}{a+z_2}-\frac{1}{a+z_1}\right]-P_1\right],$$

$$P_4(z_1,z_2)=b\left[(1-a^2)L_1+aP_1-\frac{z_2^2-z_1^2}{2}\right], \tag{A6}$$

$$P_5(z_1,z_2)=\frac{2L_1}{y\beta_W},\quad L_1=\ln\left[\frac{a+z_2}{a+z_1}\right],$$

$$a=-\frac{1+\beta_W^2}{2\beta_W},\quad b=\frac{2}{\beta_W}.$$

For the case of initial $e_R^-e_L^+(RL)$ the contributions involving the t-channel diagram (neutrino exchange) obviously vanish, while for the remaining contributions the corresponding $\bar{\sigma}^{RL}$ and $\sigma^{RL}(z_1,z_2)$ are simply obtained by replacing the g_{iL}^e's by g_{iR}^e's. The cross sections for initially LL and RR polarized e^+e^- beams identically vanish, and therefore the cross section for initially unpolarized beams is finally given by $\frac{1}{4}(\sigma^{LR}+\sigma^{RL})$. Finally, one can easily see that for $\phi=0$ one reproduces the SM expressions of cross sections originally derived in Refs. [16–18].

APPENDIX B

In this Appendix we give the explicit expressions for the couplings of the Z' to left- and right-handed fermions for the models considered in this paper.

In the presence of extra U(1)'s, the neutral current interactions are (in the mass eigenstate basis)

$$-\mathcal{L}=J_{\rm em}^{\mu}\mathcal{A}_{\mu}+J_1^{\mu}Z_{1\mu}+J_2^{\mu}Z_{2\mu}, \tag{B1}$$

where the relevant coupling constants are included in the definition of neutral currents. With $c_W=\cos\theta_W$, these constants are $e=\sqrt{4\pi\alpha_{\rm em}}$, $g_1=e/s_Wc_W$, $g_2=g_1s_W$ (for E_6 and LRM) and $g_2=g_1/\sqrt{1-2s_W^2}$ (for ALRM). In terms of the left- and right-handed projectors $P_{L,R}=(1\mp\gamma_5)/2$, the neutral current can be written as

$$J_i^{\mu}=\sum_f\bar{\psi}_f\gamma^{\mu}(g_{iL}^fP_L+g_{iR}^fP_R)\psi_f$$
$$=\sum_f\bar{\psi}\gamma^{\mu}(v_i^f-a_i^f\gamma_5)\psi_f. \tag{B2}$$

Denoting by Z,Z' the weak eigenstates as in Eq. (10), the SM $Zf\bar{f}$ couplings are the familiar ones:

$$g_L^f=(I_{3L}^f-Q^fs_W^2)g_1,\quad g_R^f=-Q^fs_W^2g_1. \tag{B3}$$

(1) For the $Z'f\bar{f}$ couplings in effective models from E_6 one has the expressions listed in Table I, where we define

TABLE I. E_6 models.

	ν	e	u	d
$g_L^{f'}/g_2$	$3A+B$	$3A+B$	$-A+B$	$-A+B$
$g_R^{f'}/g_2$	0	$A-B$	$A-B$	$-3A-B$

$$A=\frac{\cos\beta}{2\sqrt{6}},\quad B=\frac{\sqrt{10}}{12}\sin\beta, \tag{B4}$$

with β specifying the orientation of the U(1)′ generator in the E_6 group space.

(2) For the left-right models (LRM), the neutral current coupled to the Z'_{LR} can be written as

$$J_{LR}^{\mu}=\alpha_{LR}J_{3R}^{\mu}-\frac{1}{2\alpha_{LR}}J_{B-L}^{\mu}, \tag{B5}$$

where J_{3R}^{μ} is the third component of the $SU(2)_R$ isospin and B and L are the baryon and lepton numbers, respectively [right- and left-handed fermions are doublets and singlets of $SU(2)_R$ respectively, and *vice versa* for $SU(2)_L$]. The model parameter α_{LR} is defined as

$$\alpha_{LR}=\left[\frac{c_W^2}{s_W^2}\frac{g_R^2}{g_L^2}-1\right]^{1/2}, \tag{B6}$$

with $g_L=e/s_W$ and g_R the $SU(2)_R$ gauge coupling. In general, α_{LR} is taken in the range $1/\sqrt{2}\le\alpha_{LR}\le1.52$ for $s_W^2=0.23$, which corresponds to $\frac{1}{2}g_L^2\le g_R^2\le g_L^2$. However, the case most commonly considered is the left-right symmetric model (LRSM) $g_R=g_L$, corresponding to the maximum value of α_{LR}. The fermion couplings to the Z'_{LR} are reported in Table II. One can remark that for the particular value $\alpha_{LR}=\sqrt{2/3}\simeq0.83$ these couplings coincide with those of the χ model version of E_6 ($\cos\beta=1$).

(3) The alternative left-right model (ALRM) is a particular version of LRSM generated from E_6, with unconventional quantum number assignments for fermions, leading to the specific fermion couplings to the Z' listed in Table III.

APPENDIX C

We start by giving explicit expressions for the linear expansion in the mixing angle ϕ of the $e^+e^-\to f\bar{f}$ observables at the Z_2 resonance peak [see Eq. (33)]. For $\sigma_{\mu\mu}$ in (31), we can easily derive, in the same notation of (33),

$$H_{\sigma}=2(H_{\mu}-H_{\Gamma}). \tag{C1}$$

Referring to Eq. (28), Eq. (C1) holds in the approximation $\Gamma_2^{WW}\ll\sum_f\Gamma_2^{f\bar{f}}$ (recall that $\Gamma_2^{WW}\propto\phi^2$) and uses the ϕ expansion of the partial Z_2 widths into fermion species:

TABLE II. Left-right models.

	ν	e	u	d
$g_L^{f'}/g_2$	$\frac{1}{2\alpha_{LR}}$	$\frac{1}{2\alpha_{LR}}$	$-\frac{1}{6\alpha_{LR}}$	$-\frac{1}{6\alpha_{LR}}$
$g_R^{f'}/g_2$	0	$\frac{1}{2\alpha_{LR}}-\frac{\alpha_{LR}}{2}$	$-\frac{1}{6\alpha_{LR}}+\frac{\alpha_{LR}}{2}$	$-\frac{1}{6\alpha_{LR}}-\frac{\alpha_{LR}}{2}$

TABLE III. Alternative left-right model

	ν	e	u	d
$g_L^{f'}/g_2$	$-\frac{1}{2}+s_W^2$	$-\frac{1}{2}+s_W^2$	$-\frac{1}{6}s_W^2$	$-\frac{1}{6}s_W^2$
$g_R^{f'}/g_2$	0	$-\frac{1}{2}+\frac{3}{2}s_W^2$	$\frac{1}{2}-\frac{7}{6}s_W^2$	$\frac{1}{3}s_W^2$

$$\Gamma_2^{ff}=\frac{M_2}{12\pi}(v_{2f}^2+a_{2f}^2)=\Gamma_2^{ff}(0)(1+\phi H_f)\ . \tag{C2}$$

Also, Eq. (14) has been taken into account, i.e., $v_{2f}\simeq-\phi v_f+v_f'$, $a_{2f}\simeq-\phi a_f+a_f'$, so

$$H_f=-2\frac{v_f'v_f+a_f'a_f}{v_f'^2+a_f'^2}\ , \tag{C3}$$

with the Z' fermionic couplings v_f' and a_f' defined in Appendix B. Moreover, neglecting phase-space effects,

$$\Gamma_2^{ff}(0)=\frac{M_2}{12\pi}(v_f'^2+a_f'^2)\ . \tag{C4}$$

In the same approximation of identifying the total width Γ_2 to the sum over fermionic channels, we have analogously

$$\Gamma_2=\Gamma_2(0)(1+\phi H_\Gamma)\ , \tag{C5}$$

where (N_c is the color factor)

$$H_\Gamma=\frac{\sum_l H_l\Gamma_2^{ll}(0)+N_c\sum_q H_q\Gamma_2^{qq}(0)}{\sum_l\Gamma_2^{ll}(0)+N_c\sum_q\Gamma_2^{qq}(0)}\ . \tag{C6}$$

For the expansion of R' defined in (31),

$$R'=R'(0)(1+\phi H_{R'})\ , \tag{C7}$$

one finds, by the same procedure,

$$H_{R'}=H_h-H_\mu\ , \tag{C8}$$

with

$$H_h=\frac{\sum_q H_q\Gamma_2^{qq}(0)}{\sum_q\Gamma_2^{qq}(0)}\ . \tag{C9}$$

For asymmetries, which are relative quantities, we write the ϕ expansions as

$$A_{LR}=A_{LR}(0)+\phi H_{LR} \tag{C10}$$

for both leptonic and hadronic final states, with

$$H_{LR}=-2\Delta A_l \tag{C11}$$

and

$$\Delta A_l=2\frac{v_l'a_l'(v_lv_l'+a_la_l')}{(v_l'^2+a_l'^2)^2}-\frac{v_l'a_l+v_la_l'}{v_l'^2+a_l'^2}\ . \tag{C12}$$

Moreover,

$$A_{LR}(0)=-2\frac{v_l'a_l'}{v_l'^2+a_l'^2}\ . \tag{C13}$$

Finally, limiting to the leptonic channel,

$$A_{FB}^{\mu}=A_{FB}^{\mu}(0)+\phi H_{FB}\ , \tag{C14}$$

where [referring to Eq. (31)]

$$H_{FB}=6A_l(0)\Delta A_l \tag{C15}$$

and

$$A_{FB}^{\mu}(0)=3[A_l(0)]^2\ . \tag{C16}$$

For large values of M_2, of the order of 1 TeV or larger, it turns out that one should use for Γ_2 the full Eq. (28), accounting also for the contribution of Γ_2^{WW}. The latter is

$$\Gamma_2^{WW}=\frac{M_2}{12\pi}\left[\frac{M_2}{M_W}\right]^4\left[\frac{e}{\tan\theta_W}\right]^2\sin^2\phi \times\frac{1}{16}\left[1-4\frac{M_W^2}{M_2^2}\right]^{3/2}\left[1+20\frac{M_W^2}{M_2^2}+12\frac{M_W^4}{M_2^4}\right]\ . \tag{C17}$$

Then Eq. (C5) changes to

$$\Gamma_2=\sum_f\Gamma_2^{ff}(0)\left[1+\phi H_\Gamma+\frac{\Gamma_2^{WW}}{\sum_f\Gamma_2^{ff}(0)}\right]\ . \tag{C18}$$

[1] For a review and a list of references see J. L. Hewett and T. G. Rizzo, Phys. Rep. **183**, 194 (1989).

[2] P. Chiappetta *et al.*, in *Proceedings of the ECFA Large Hadron Collider Workshop,* Aachen, Germany, 1990, edited by G. Jarlskog and D. Reen (CERN Report No. 90-10, Geneva, Switzerland, 1990), Vol. II, p. 685.

[3] R. M. Barnett *et al.*, in *High Energy Physics in the 1990's,* Proceedings of the Summer Study, Snowmass, Colorado, 1988, edited by S. Jensen (World Scientific, Singapore, 1989).

[4] A. Djouadi, A. Leike, T. Riemann, D. Schaile, and C. Verzegnassi, Z. Phys. C **56**, 289 (1992).

[5] G. Altarelli, in Electroweak Interactions and Unified Theories, Proceedings of the 27th Rencontre de Moriond, Les Arcs, France, 1992 (unpublished).

[6] G. Altarelli, R. Casalbuoni, S. De Curtis, N. Di Bartolomeo, F. Feruglio, and R. Gatto, Phys. Lett. B **263**, 459 (1991).

[7] P. Langacker and M. Luo, Phys. Rev. D **45**, 278 (1992).

[8] J. Layssac, F. M. Renard, and C. Verzegnassi, Z. Phys. C **53**, 97 (1992); Phys. Lett. B **287**, 267 (1992).

[9] A. A. Pankov and N. Paver, Phys. Lett. B **272**, 425 (1991); **274**, 483 (1992).

[10] A. A. Pankov and I. S. Satsunkevich, Yad. Fiz. **47**, 1333 (1988) [Sov. J. Nucl. Phys. **47**, 849 (1988)]; Nuovo Cimento **103A**, 1121 (1990).

[11] A. A. Pankov and C. Verzegnassi, Phys. Lett. B **233**, 259 (1989).

[12] S. S. Gershtein, A. A. Likhoded, A. A. Pankov, and O. P. Yushchenko, Phys. Lett. B **275**, 169 (1992); Z. Phys. C **56**, 279 (1992).

[13] F. Boudjema, B. W. Lynn, F. M. Renard, and C. Verzegnassi, Z. Phys. C **48**, 595 (1990).

[14] For a review and references, see R. N. Mohapatra, *Unification and Supersymmetry* (Springer, New York, 1986).

[15] See, e.g., V. Barger and K. Whisnant, Int. J. Mod. Phys. A **3**, 879 (1988), and references therein.

[16] P. Sushkov, V. V. Flambaum, and I. B. Khriplovich, Yad. Fiz. **20**, 1016 (1975) [Sov. J. Nucl. Phys. **20**, 537 (1975)].

[17] W. Alles, Ch. Boyer, and A. J. Buras, Nucl. Phys. **B119**, 125 (1977).

[18] R. W. Brown and K. O. Michaelian, Phys. Rev. D **19**, 922 (1979).

[19] For a detailed discussion see, e.g., D. Burke, in *Gauge Bosons and Heavy Quarks,* Proceedings of the Eighteenth SLAC Summer Institute on Particle Physics, Stanford, California, 1990, edited by J. Hawthorne (SLAC Report No. 378, Stanford, 1991), p. 97.

[20] V. Barger, N. G. Deshpande, J. L. Rosner, and K. Whisnant, Phys. Rev. D **35**, 2893 (1987).

[21] J. A. Grifols, A. Méndez, and R. M. Barnett, Phys. Rev. D **40**, 3613 (1989).